Magnetic structure of the spin-density wave antiferromagnet CaFe_{4}As_{3} from magneto-elastic coupling

Mario Poirier, Marie Anne Richard, Jérémie Pilon, Amar B. Karki, and Rongying Jin

Phys. Rev. B **87**, 014407 — Published 7 January 2013

DOI: 10.1103/PhysRevB.87.014407

Magnetic structure of the spin-density wave antiferromagnet $CaFe_4As_3$ from magneto-elastic coupling

Mario Poirier[1], Marie Anne Richard[1], Jérémie Pilon[1], Amar B. Karki[2], and Rongying Jin[2]
[1]*Regroupement Québécois sur les Matériaux de Pointe, Département de Physique, Université de Sherbrooke, Sherbrooke, Québec, Canada J1K 2R1 and*
[2]*Department of physics and astronomy, Louisiana State University, Baton Rouge, Louisiana 70803, USA*
(Dated: November 27, 2012)

We report an ultrasonic study of the magneto-elastic coupling of the spin-density wave antiferromagnet $CaFe_4As_3$. Longitudinal waves propagating along the $\boldsymbol{a}$ axis reveal anomalies on the acoustic velocity at both the incommensurate (ICM) (T_{N1} = 89.3 K) and commensurate (CM) (T_{N2} = 26.3 K) spin-density phases, which are consistent with the magnetic structure established from neutron diffraction experiments. Moreover, at higher temperatures, magnetic fluctuations are likely responsible for a reduced stiffening of the velocity below 150 K. Although the ICM phase appears elastically inhomogeneous below 50 K, a precise magnetic field dependence of the ICM-CM transition at T_{N2} specifies a preferential orientation of the in-plane easy and hard axes respectively parallel and perpendicular to the vector $\hat{\boldsymbol{d}}$ ($\hat{\boldsymbol{a}} \cdot \hat{\boldsymbol{d}} = \cos 30°$). Within the CM phase, a magnetic field aligned along the ribbon $\boldsymbol{b}$ axis reveals a new magnetic transition of the *spin-flop* type near 16 teslas. For this particular field direction a phase diagram is proposed.

PACS numbers: 75.30.Fv,72.55.+s,73.50.Rb

I. INTRODUCTION

The recent discovery of superconductivity in Fe-As-based materials has accelerated the search for new compounds constructed with the same building block, i.e. edge-shared $FeAs_4$ tetrahedron, in view of establishing correlation between crystal structure, magnetism and superconductivity. In the so-called parent compounds of these layered-(Fe-As)-based superconductors, there are two successive phase transitions. One is the structural phase transition at T_s from tetragonal at high temperatures to orthorhombic at low temperatures. The other is the long-range three-dimensional antiferromagnetic (AFM) spin density wave (SDW) order at T_N, with T_s slightly higher or equal to T_N[1]. Below $T_N \approx 130$ - 220 K, a Fe^{2+} moment is aligned within the layer (ab) plane[1,2]. By introducing chemical doping (or hydrostatic pressure), both the structural and magnetic transitions are suppressed and superconductivity emerges above a critical concentration dependent on the substituent[3,4].

While strong magneto-elastic (magneto-phonon) coupling in these layered compounds has been theoretically predicted[5–8], it is difficult to experimentally probe the spin-dependent phonon modes because of the coupled structural and magnetic transitions. Due to large T_N, the magnetic field available for experimental techniques such as neutron scattering and Raman spectrometer is insufficient to separate T_s and T_N. A more effective way is to study magnetophonon coupling in a Fe-As-based compound that does not have such coupled structural and magnetic transitions. For this purpose, the new compound $CaFe_4As_3$ is the ideal material. It has the orthorhombic structure up to at least room temperature, where $FeAs_4$ tetrahedra form ribbons along the $\boldsymbol{b}$ axis and a rectangular network in the $\boldsymbol{ac}$ plane[9–11]. These interpenetrating Fe-As ribbons, which are connected by fivefold coordinated Fe^{1+} sites forming channels which host the Ca atoms, may provide unique insight into the electronic correlations of the square lattice. Yet, the system undergoes two successive AFM-SDW transitions[9,10], a longitudinal incommensurate spin density wave (ICM-SDW) at $T_{N1} \sim 90$ K along the $\boldsymbol{b}$ axis and a transverse commensurate spin density wave (CM-SDW) at $T_{N2} \sim 26$ K in the $\boldsymbol{ac}$ plane[12–14]. The magnetization is anisotropic with larger values along the ribbons ($\parallel \boldsymbol{b}$) and the large Sommerfeld constant indicates relatively strong electronic correlations[10,14]. The IC-SDW transition at T_{N1} is second-order with a modulation wavevector $\mathbf{k} = (0, \delta, 0)$ varying in the range $0.375 < \delta < 0.390$[12,13]; this phase could result from competing second and third order nearest-neighbor (NN) interactions in the localized spin picture. The commensurate to incommensurate (CM-ICM) transition at T_{N2} is first-order with a wavevector lock-in at $\delta = \frac{3}{8}$[12,13]; although the transition is associated to the development of a transverse component, the magnetic moments remain predominantly aligned along the $\boldsymbol{b}$ axis. Density functional theory calculations suggest that nesting plays a role in the CM transition[13]. These two magnetic phase transitions have been detected trough several anomalies in bulk properties. In particular, the sudden drop of the electrical resistivity at T_{N2} associated with a surprisingly weak anomaly in the heat capacity were explained by the presence of a sixteenth degree invariant in the Landau energy that stabilizes the CM phase[12].

In this paper, we precise the magnetic structure of $CaFe_4As_3$ by probing the magneto-elastic coupling in a single crystal with an ultrasonic propagation technique. Longitudinal acoustic waves propagating along the $\boldsymbol{a}$ axis reveal well-defined anomalies in the temperature profile of the velocity that are associated with both magnetic transitions at T_{N1} and T_{N2}. Moreover, a reduced stiffening of the velocity below 150 K could result from magnetic fluctuations preceding the ICM phase transition. A magnetic field investigation of the elastic anomaly at the CM-ICM phase transition at T_{N2} confirms that $CaFe_4As_3$ can be considered as an uniaxial antiferromagnet with a first-order spin-flop (SF) transition along the ribbon $\boldsymbol{b}$ axis and an in-plane ($\boldsymbol{ac}$) anisotropy with easy and hard axes preferentially oriented along directions rotated by 30° from the crystal axes. A magnetic phase diagram is then proposed.

II. EXPERIMENT

Single crystals of $CaFe_4As_3$ were grown out of the Sn flux[14] as needles oriented along the ribbons axis $\boldsymbol{b}$. Their structure was determined from x-ray diffraction which confirmed the orthorhombic space-group symmetry *Pnma*. The crystal used for the ultrasonic experiment was one of the few crystals of the same batch showing natural parallel faces (perpendicular to the $\boldsymbol{a}$ axis) and sufficient thickness that are both required in our ultrasonic method. We use a pulsed ultrasonic interferometer to measure the variation of the longitudinal acoustic velocity along the crystal direction $\boldsymbol{a}$ relative to the value at T_0, $\Delta V/V = [V(T) - V(T_0)]/V(T_0)$. The acoustic pulses are generated with $LiNbO_3$ piezoelectric transducers resonating at 30 MHz and odd overtones bonded to the crystals with silicone seal. Since the crystal structure is orthorhombic, the velocity is related to the C_{11} elastic constant or compressibility modulus through the relation $C_{11} = \rho V^2$, where ρ is the density. The ultrasonic technique is used in the transmission mode and, because of the reduced thickness of the crystal along the $\boldsymbol{a}$ axis (~ 0.25 mm), a CaF_2 delay line must be used to separate the first transmitted acoustic echo from the electric pulse. Moreover, no transverse acoustic mode can be properly analyzed because of mode conversion and mode mixing at the different interfaces. The longitudinal mode can be measured because it has the largest velocity that permits its time separation from parasitic signals. The $\Delta V/V$ data are directly the image of the relative variation of the compressibility modulus C_{11} if both the density and the sample's length changes can be neglected, an assumption that is generally verified in such materials. The temperature was varied between 2 and 200 K and a magnetic field up to 16-18 teslas could be oriented along the different crystal axes.

We checked the quality of our crystals by using a standard microwave cavity perturbation technique[15] operated in the TE_{102} mode at 16.5 GHz. After insertion of the needle shaped crystal in the cavity electric field, we measure changes in the relative complex resonance frequency shift, $(\Delta f/f + i\Delta(1/2Q)) = (\delta + i\Delta/2)$, ($Q$ is the cavity quality factor) as a function of temperature and magnetic field. According to the known value of the resistivity of these crystals[14] and the thickness of our sample, these data should be treated in the skin depth regime or the surface impedance approximation for which the dissipation term $\Delta/2$ is compared to the corrected frequency shift $(\alpha/N + \delta)$, α and N are respectively the cavity filling and the depolarization factors[16]. The geometrical factor α/N represents then the relative frequency shift obtained with infinite electrical conductivity. In the skin depth regime, the resistivity is proportional to $(\Delta/2)^2$.

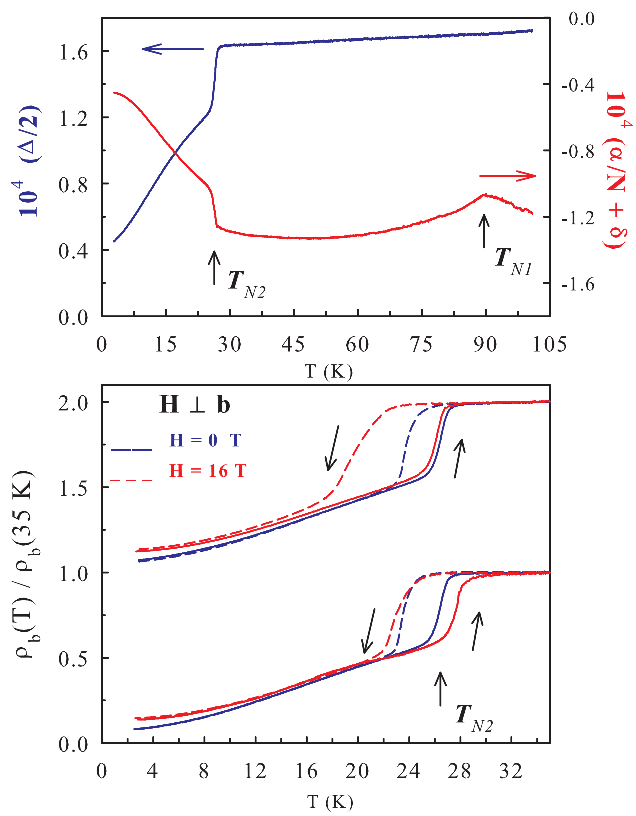

FIG. 1: (Color online) Complex relative frequency shift at 16.5 GHz (upper panel) as a function of increasing temperature and normalized microwave resistivity (lower panel) as a function of temperature (cooling and warming cycles indicated by arrows) for a magnetic field H = 0 (blue) and 16 T (red), the field being oriented along two different *unknown* directions within the $\boldsymbol{ac}$ plane. In the lower panel, one set of curves has been shifted up to help the comparison.

III. RESULTS AND DISCUSSION

To facilitate the forthcoming discussion of the elastic properties of $CaFe_4As_3$, it is important to verify that the electronic properties of our crystals are similar to the ones found in the literature[14]. Thus, using a contact-free technique, we measured the microwave resistivity on a crystal taken from the same batch used for the ultrasonic experiment. The microwave electric field was oriented along the needle $\boldsymbol{b}$ axis to minimize the depolarization field. We present in figure 1 (upper panel) the temperature dependence of both parts of the complex frequency shift below 105 K. In the surface impedance regime, we should expect $\Delta/2 = -(\alpha/N + \delta)$ which is not obviously the case over this temperature range, at least above $T_{\rm N2}$. The ICM transition at $T_{\rm N1} = 89.3(1)$ K is identified as a sharp cusp on $-(\alpha/N+\delta)$ when a small slope variation is hardly observed on the losses $\Delta/2$. At $T_{\rm N2} = 26.3(1)$ K (determined from the maximum temperature derivative), the CM-ICM transition produces a sharp drop of both parts of the frequency shift. The real part $-(\alpha/N + \delta)$ is related to the electromagnetic field penetration depth: an increase below $T_{\rm N1}$ is consistent with enhanced resistivity due to a partial gapping of the Fermi surface when the rapid decrease below $T_{\rm N2}$ is due to reduced spin scattering in the CM phase[14]. The losses $\Delta/2$ follow the same picture but they are directly related to the resisitivity ρ_b along the $\boldsymbol{b}$ axis which, in the skin depth regime, is proportional to $(\Delta/2)^2$[16].

To avoid uncertainties on the absolute value of ρ_b related to the evaluation of the geometrical factors α and N, we present in figure 1 (lower panel) the normalized resistivity below 35 K. In zero magnetic field, the temperature profile is very similar to the low frequency resistivity data[14] and the first-order character of the transition is clearly established by the hysteresis loop during a warming-cooling cycle. In our microwave experiment, a magnetic field can be applied along a direction perpendicular to the needle axis within the $\boldsymbol{ac}$ plane. The normalized resistivity data in a field of 16 T are shown in figure 1 for two unknown in-plane orientations (two different experiments on the same sample). If the field effects on the resistivity at low temperatures are similar to published data[14], the shift of $T_{\rm N2}$ with field is found to depend on the exact orientation of the field within the plane, positive for the lower curves and negative for the upper ones. The amplitude of the hysteresis loop appears also to scale with the $T_{\rm N2}$ shift, a larger amplitude being associated to negative temperature shift (upper curves). If we except these novel *in-plane anisotropic* magnetic field effects, our microwave data are fully consistent with published low frequency data and confirm the quality of the crystals.

When temperature is decreased below room temperature, the elastic moduli of solids usually increases due to the strengthening of the bonds between atoms and saturate at low temperatures. At constant crystal density, this yields a progressive stiffening of the acoustic velocity for $\rm CaFe_4As_3$ as shown in figure 2 at two ultrasonic frequencies. Superposed on this stiffening background, we observed two well-defined elastic anomalies at the magnetic phase transitions at $T_{\rm N1}$ and $T_{\rm N2}$ and another anomaly signals a reduction in the stiffening rate below a crossover temperature $T_{\rm M} \sim 155$ K. The small differences observed between the two frequencies are believed to be due to the reduced thickness of the samples which does not allow a complete time separation of multiple reflected pulses inside the crystal and thus perturbs the constant phase method of the interferometer.

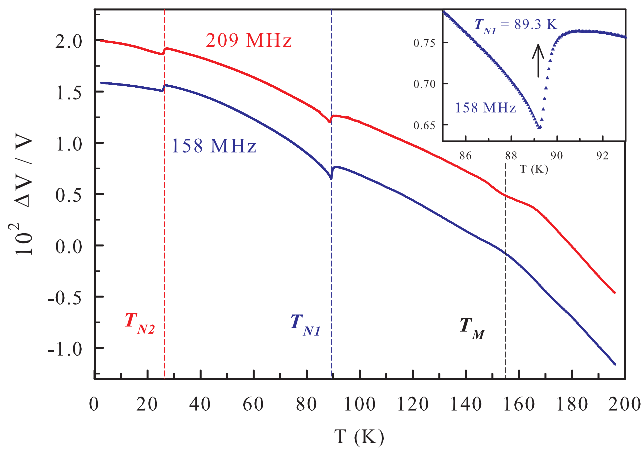

FIG. 2: (Color online) Temperature dependence of the relative variation of the longitudinal velocity $\Delta V/V$ along the $\boldsymbol{a}$ axis below 200 K at 158 and 209 MHz. The dashed lines indicate transition and crossover temperatures. Inset: zoom on the elastic anomaly at 158 MHz in the vicinity of the ICM transition at $T_{\rm N1}$.

The reduced stiffening below $T_{\rm M}$ could be due to magnetic fluctuations preceding the ICM phase transition. Spins are known to couple easily to strain in various magnetic systems so as to induce a monotonic softening on the compressibility modulus whose temperature dependence correlates with the regular increase of magnetic susceptibility with temperature above the transition temperature. For weakly coupled insulating spin chains for example[17,18], the softening upon warming presents a maximum at a temperature comparable to the spin exchange constant namely, $T \approx J/k_B$, in agreement with the characteristic temperature for the maximum in the temperature dependent spin susceptibility[19]. The situation is somewhat different for $\rm CaFe_4As_3$ since we probe the compressibility modulus perpendicular to the ribbons for which the magneto-elastic coupling is expected to be smaller. Moreover, the maximum of the elastic softening could be masked by the outcome of the ICM phase. This reduced stiffening occurs over the same temperature range where an unusual behavior of thermal transport properties along the $\boldsymbol{b}$ axis was observed and possibly attributed to magnetic fluctuations[14]. Evidence for spin fluctuations was also observed via Mössbauer spectroscopy[20].

As shown in the inset of figure 2 the velocity softens rapidly as the ICM phase transition at $T_{\rm N1}$ is approached from above. This softening is likely the result of three-dimensional magnetic fluctuations due to increased coupling between ribbons. Maximum softening is obtained at $T_{\rm N1} = 89.3(3)$ K below which the velocity stiffens with an enhanced rate. Since there is no structural change at the magnetic transition, the enhancement of the rate is due to a magneto-elastic coupling between the modulation (of wavevector $\mathbf{q}$) proportional to the magnetic gap Δ_q and the uniform elastic deformation e[21]. There is no possibility to extract the magnetic gap here because of the unknown normal elastic background. The absence of thermal hysteresis confirms the second-order character of the ICM transition. When a transverse magnetic field has no measurable effects on the transition temperature T_{N1}, a decrease is observed for a longitudinal one as discussed later.

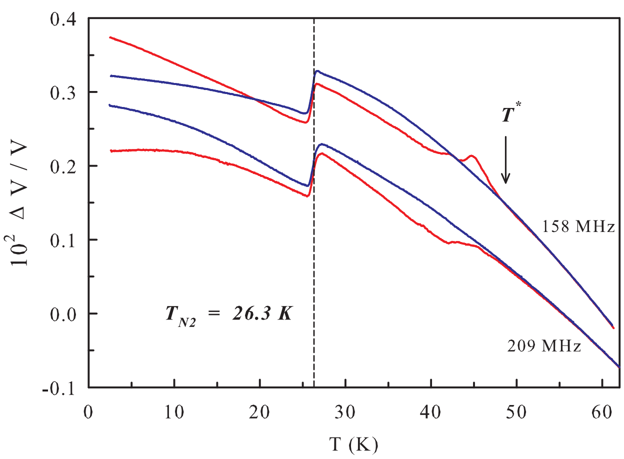

FIG. 3: (Color online) Temperature dependence of the relative variation of the velocity $\Delta V/V$ along the $\boldsymbol{a}$ axis below 60 K at 158 and 209 MHz. The dashed line indicates the CM-ICM transition temperature T_{N2}. First warming cycle to 60 K after cooling from 200 K (red curves) and second warming cycle after cooling from 60 K (blue curves).

The temperature range below 60 K where the CM-ICM transition is found at $T_{\mathrm{N2}} = 26.3(2)$ K (determined as the maximum in the negative temperature derivative) is examined in figure 3 for two different warming cycles. On all curves, the CM-ICM transition produces a sharp softening whose amplitude appears independent of frequency and, in particular, of thermal cycle. However, we observe below $T^* \sim 50$ K an inhomogeneous elastic behavior as the CM-ICM phase transition is approached. This unusual behavior is mainly observed during the first warming cycle to 60 K after having cooled the sample from 200K (red curves); when the sample is subsequently cooled back to 2 K and warmed to 60 K (second warming cycle, blue curves), the temperature profile below T^* has been smoothed and it does not change much during subsequent thermal cycling to 60 K. This inhomogeneous elastic behavior is weakly frequency dependent as expected but it affects neither the value of T_{N2} nor the amplitude of the softening at the CM-ICM transition. Such an instability of the ICM phase below T^* has not yet been observed on transport, thermodynamic or magnetic properties. All the data discussed in this work were obtained after a few warming cycles to 60 K (including figure 2) to minimize this elastic instability.

We now investigate the magnetic structure of the CM phase by studying the magnetic field dependence of the softening anomaly appearing at T_{N2}. We begin with the magnetic field oriented within the $\boldsymbol{ac}$ plane that should show anisotropic effects if we believe the microwave resistivity data (Fig.1). We compare in figure 4 the temperature dependence of the velocity data below 60 K obtained in zero and 16 T fields applied along the two directions $\hat{\mathbf{d}}$ ($\hat{\mathbf{a}}\cdot\hat{\mathbf{d}} = \cos\theta$) that show upon warming maximum positive ($\theta = 30°$) and negative ($\theta = 120°$) shifts of the transition temperature T_{N2}. During the cooling cycle from 60 K, the velocity curves begin to separate from the warming ones below 50 K and the usual hysteretic effects occur at the CM-ICM transition (downshift of T_{N2}); we notice that the lower the transition temperature, the wider the hysteresis loop.

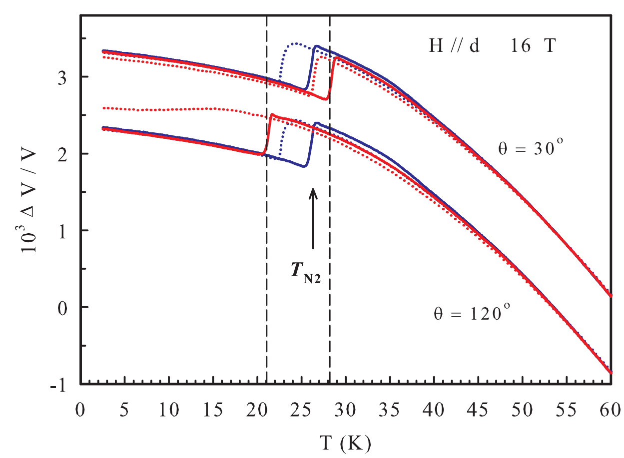

FIG. 4: (Color online) Temperature dependence of the relative variation of the velocity $\Delta V/V$ along the $\boldsymbol{a}$ axis below 60 K at 158 MHz in zero (blue) and 16 teslas (red) magnetic field values: warming (continuous lines) and cooling (dotted lines) cycles. The field is oriented along the vector $\hat{\mathbf{d}}$ ($\hat{\mathbf{a}} \cdot \hat{\mathbf{d}} = \cos\theta, \theta = 30°, 120°$). The two sets of data have been shifted vertically from one another to facilitate the discussion. The dashed lines indicate the shift of the transition temperature relative to the zero field value indicated by an arrow.

The in-plane anisotropy of the CM-ICM transition suggested by the microwave experiment is thus confirmed by the elastic data. We show in figure 5 the transition temperature T_{N2} measured at 16 T as a function of the angle θ. Starting from the $\boldsymbol{a}$ axis, the temperature is progressively shifted to higher temperatures and nearly saturates near 28.3 K over a wide range of angles centered around $\theta = 30°$ where a small dip is observed; as the angle is further increased toward the $\boldsymbol{c}$ axis, T_{N2} decreases, intersects the zero-field value $T_{N2}(0)$ and reaches a minimum value of 21.0 K at 120°, a temperature shift of nearly 20%! These results suggest that the CM phase is the most stabilized to the detriment of the ICM one when the magnetic field is oriented 30° from the $\boldsymbol{a}$ axis; the re-

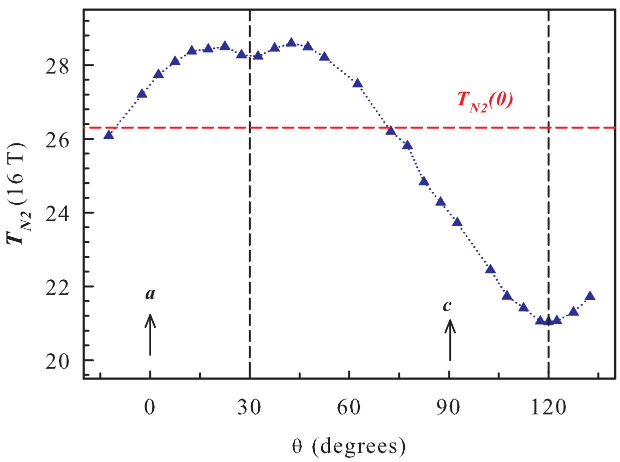

FIG. 5: (Color online) Shift of the CM-ICM transition temperature T_{N2} in a field of 16 T as a function of the angle θ within the $\boldsymbol{ac}$ plane. The horizontal dashed line indicates the transition temperature $T_{N2}(0)$ in zero field.

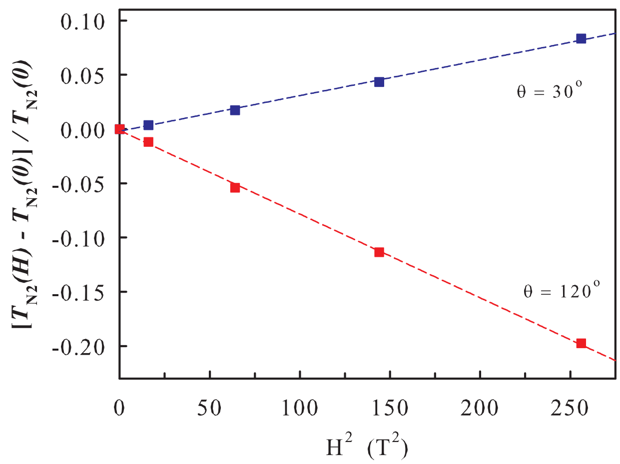

FIG. 6: (Color online) Magnetic field dependence of the CM-ICM transition temperature T_{N2} for the warming cycle for the two in-plane orientations $\theta = 30°$ and $120°$. The dashed lines are the fit to eq.1.

verse outcome is obtained for the 120° orientation. These observations within the CM phase could be explained by the existence of a magnetic anisotropy term that favors the preferential alignment of the transverse component of the Fe moments along a direction 30±15 degrees from the $\boldsymbol{a}$ axis, which can thus be considered as an in-plane easy-axis. Coherently, the hard-axis is attributed to the narrow range of angles at the 120° direction. However, this magnetic structure could only be validated by the precise identification of the magnetic anisotropy term. We have plotted in figure 6 the relative variation of the CM-ICM transition temperature, $[T_{N2}(H) - T_{N2}(0)]/T_{N2}(0)$, as a function of the square of the magnetic field. For both orientations, the variation with field follows the quadratic dependence

$$T_{\mathrm{N2}}(H) = T_{\mathrm{N2}}(0)\left[1 + cH^2\right], \qquad (1)$$

with a constant $c = +0.33\ 10^{-3}$ and - $0.77\ 10^{-3}$ tesla^{-2} respectively for $\theta = 30°$ and 120°. Finally, we notice that the temperature profiles of the velocity data are affected by the magnetic field below 50 K where the warming and cooling curves split from each other (Fig.4); this may signify that the inhomogeneous elastic behavior below 50 K could be due to precursor effects of the CM-ICM transition. The elastic softening occurring at T_{N2} can be explained by a reduction of either the magnetic gap (due to a change in wavevector) or the magneto-elastic coupling constant. No clear answer is available at this moment.

We now examine in figure 7 the effects of a magnetic field oriented along the ribbon $\boldsymbol{b}$ axis. Below 16 T, the field merely shifts T_{N2} to higher temperatures without affecting much the overall temperature dependence of the velocity with a consistent decrease of the hysteresis loop amplitude (similarly to the in-plane measurements of Fig.4 at $\theta = 30°$). However, a new elastic anomaly is surprisingly observed when the field is increased above 16 T as shown in figure 7 for different field values during warming cycles. At 16 T, besides the usual softening anomaly at the CM-ICM phase transition, whose amplitude is not dependent on field, an additional softening anomaly is detected below T_{N2} near 6 K. With increasing field, the anomaly grows as a very sharp dip moving rapidly to higher temperatures (vertical arrows). The anomaly's amplitude is much larger than the one at T_{N2} and it peaks around H = 16.5 T before progressively decreasing as it approaches the CM-ICM transition. Hysteretic effects are observed on this anomaly as shown in the inset of Fig.7 where both the dip's position and amplitude are modified accordingly between the warming and cooling cycles. The behavior of this anomaly with temperature and magnetic field is very similar to the one observed at a *spin-flop* (SF) transition which is a field-driven first-order reorientation transition in easy-axis antiferromagnets[22,23].

We present in figure 8 two results that are also typically associated to a SF transition. In Fig.8A we show a field scan of the anomaly at 5.2 K that presents a very sharp dip near H = 16 T as expected for a SF transition. When the direction of the field is moved away from the $\boldsymbol{b}$ axis (toward $\boldsymbol{c}$), the dip amplitude decreases rapidly with the angle ϕ in a symmetrical fashion as shown in Fig.8B, for example, at T= 5.2 K and H = 16 T. The anomaly can be observed only in a small ±5° range of angles around the easy-axis $\boldsymbol{b}$. Thus, the elastic data confirm that, within the CM phase, $CaFe_4As_3$ behaves as an easy-axis antiferromagnet where the Fe moments are predominantly aligned along the ribbon axis with a small transverse component oriented preferentially 30° from the $\boldsymbol{a}$ axis, in perfect agreement with the neutron

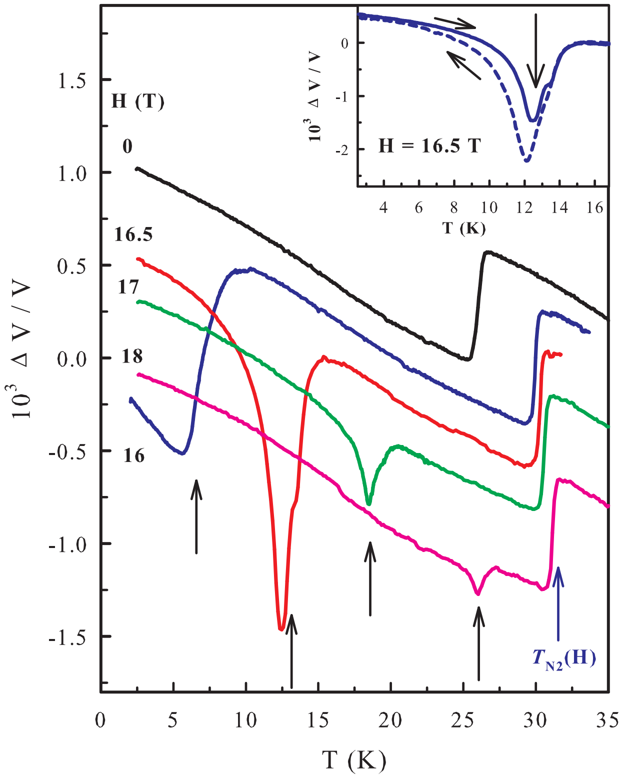

FIG. 7: (Color online) Temperature dependence of the relative variation of the velocity $\Delta V/V$ along the $\boldsymbol{a}$ axis below 35 K at 158 MHz for a magnetic field oriented along the $\boldsymbol{b}$ axis. The curves have been shifted vertically relative to the zero field value. The vertical arrows indicate the SF anomaly. Inset: hysteretic effects upon warming and cooling cycles at H = 16.5 T.

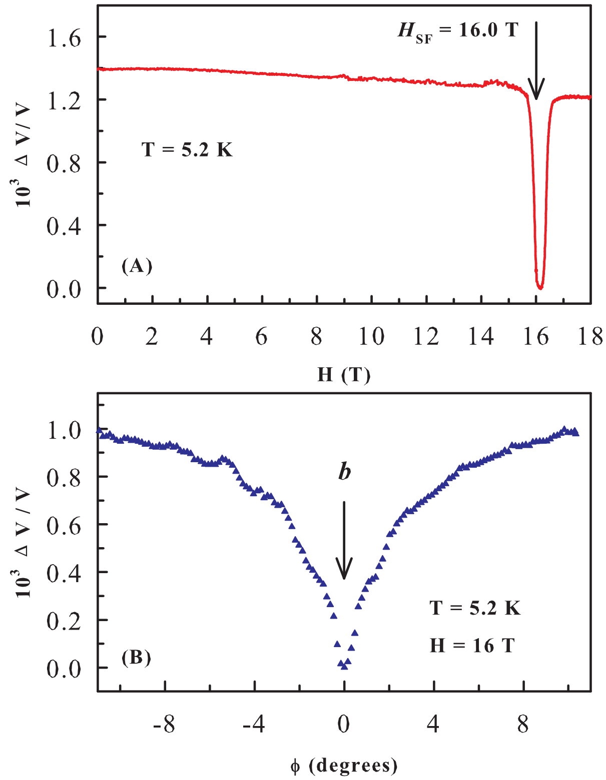

FIG. 8: (Color online) Elastic spin-flop anomaly at 5.2 K: (A) magnetic field dependence along the $\boldsymbol{b}$ axis; (B) orientational dependence relative to the $\boldsymbol{b}$ axis at H = 16 T, ϕ being the angle between $\boldsymbol{b}$ and $\boldsymbol{c}$.

scattering experiments[13] although no specific in-plane orientation is mentioned.

With the elastic data obtained for a field along the $\boldsymbol{b}$ axis, we have constructed the magnetic phase diagram shown in figure 9. When the CM-ICM transition at T_{N2} is shifted to higher temperatures with increasing field (more than 6 K at 18 T), the incommensurate to paramagnetic transition (ICM-PM) at T_{N1} is rather shifted down; we remind that a transverse field had no measurable effects on T_{N1}. Over the complete magnetic field range, both transition lines $T_{N1}(H)$ and $T_{N2}(H)$ present a very similar power law exceeding the usual quadratic dependence.

$$T_{N1}(H) = T_{N1}(0)\left[1 - (1.3\ 10^{-5})\ H^{2.47}\right], \qquad (2)$$

$$T_{N2}(H) = T_{N2}(0)\left[1 + (2.4\ 10^{-4})\ H^{2.33}\right], \qquad (3)$$

These field variations indicate clearly a stabilization of the CM phase by a longitudinal magnetic field to the detriment of the ICM one. The SF phase appears above a critical field $H_{SF}(0)$ = 15.75 T and, differently from other uniaxial antiferromagnets[22,23], the SF field $H_{SF}(T)$ increases significantly according to the relation

$$H_{SF}(T) = H_{SF}(0)\left[1 + (1.1\ 10^{-3})\ T^{1.5}\right], \qquad (4)$$

until it appears to join with the $T_{N2}(H)$ line. As indicated on Fig.9, the extrapolated $H_{SF}(T)$ and $T_{N2}(H)$ fitted lines suggest the probable existence of a multicritical point near (T_{crit}, H_{crit}) = (31.5 K, 18.5 T). However, the novelty and nature of this critical point could only be disclosed with higher field values which are currently not available from our ultrasonic set-up. This phase diagram should be taken into account for the development of an appropriate theoretical model and for programming neutron diffraction measurements that are essential to the complete characterization of the magnetic structure.

IV. CONCLUSION

In this work, we have shown that Fe magnetic moments in $CaFe_4As_3$ couple substantially with low frequency longitudinal elastic waves propagating along the crystal axis $\boldsymbol{a}$, so that it modifies the overall temperature profile of their velocity. A softening anomaly at the second-order

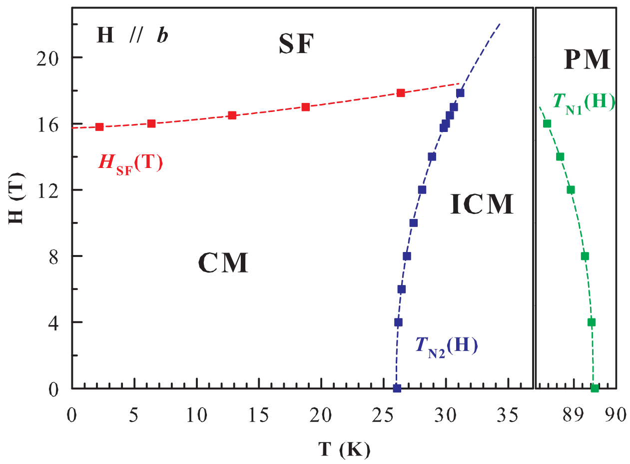

FIG. 9: (Color online) Magnetic phase diagram of $CaFe_4As_3$ for $\mathbf{H}//\boldsymbol{b}$. Commensurate (CM), Incommensurate (ICM), Spin-Flop (SF) and Paramagnetic (PM) phases. The dashed lines represent the best fits to a power law: spin-flop field $H_{\rm SF}(T)$ (red), CM-ICM transition temperature $T_{\rm N2}(H)$ (blue) and ICM-PM transition temperature $T_{\rm N1}(H)$ (green). The dashed lines (red and blue) cross at a critical point ($T_{\rm crit}$, $H_{\rm crit}$) = (31.5 K, 18.5 T).

ICM-PM transition followed by an enhanced stiffening below $T_{\rm N1} = 89.3$ K is consistent with 3D magnetic fluctuations followed by the outcome of magnetic order parameter Δ_q. A sharp softening anomaly at $T_{\rm N2} = 26.3$ K, that does not affect the overall temperature dependence of the velocity in this temperature range, confirms the first-order character of the CM-ICM transition; this anomaly could be due to a reduction of the Δ_q amplitude and/or of the magneto-elastic coupling constant. When these observations are coherent with the magnetic properties deduced from neutron diffraction experiments, novel features allow to precise the magnetic structure of this compound. Magnetic fluctuations along the ribbon axis, which precede the ICM transition, are likely responsible for a reduction of the velocity stiffening below 155 K and possibly for the unusual thermal properties. An inhomogeneous elastic behavior below 50 K, within the ICM phase, are considered precursory effects to the first-order CM-ICM transition, effects that appear to be absent on transport and magnetic properties. A magnetic field study of the elastic anomalies has revealed that $CaFe_4As_3$ is associated to an easy-axis antiferromagnet: a magnetic field oriented along the ribbon axis drives a first-order reorientation transition, or spin-flop transition, above a critical value around 16 T, and a transverse field reveals, within the plane, easy- and hard-axes that are rotated by 30° from the crystal ones. Finally, we have constructed a phase diagram that hopefully will foster the development of a unifying theoretical model.

Acknowledgments

The authors thank Janice Musfeldt to have initiated the collaboration leading to this project and acknowledge the technical support of Mario Castonguay. This work was supported by grants from the Fonds Québécois de la Recherche sur la Nature et les Technologies (FQRNT), the Natural Science and Engineering Research Council of Canada (NSERC), and US NSF through DMR-1002622.

[1] For a review, see M. D. Lumsden and A. D. Christianson, J. Phys.: Cond. Matt. **22**, 203203 (2010).
[2] Q. Hyang, Y. Qiu, Wei Bao, M.A. Green, J.W. Lynn, Y.C. Gasparovic, T. Wu, G. Wu and X.H. Chen, Phys. Rev. Lett. **101**, 257003 (2008).
[3] N. Ni, A. Thaler, J.Q. Yan, A. Kracher, E. Colombier, S.L. Bud'ko and P.C. Canfield, Phys. Rev. B **82**, 024519 (2010).
[4] A.P. Dioguardi, N. Roberts-Warren, A.C. Shockley, S.L. Bud'ko, N. Ni, P.C. Canfield and N.J. Curro, Phys. Rev. B **82**, 140411(R) (2010).
[5] Z. P. Yin, S. Lebegue, M. J. Han, B. P. Neal, S. Y. Savrasov, W. E. Pickett, Phys. Rev. Lett. **101**, 047001 (2008).
[6] E. Akturk, S. Ciraci, Phys. Rev. B **79**, 184523 (2009).
[7] T. Yildirim, Phys. Rev. Lett. **102**, 037003 (2009).
[8] I. I. Mazin, M. D. Johannes, Nature Phys. **5**, 141 (2009).
[9] , I. Todorov, D.Y. Chung, C.D. Malliakas, Q. Li, T. Bakas, A. Douvalis, G. Trimarchi, K. Gray, J.F. Mitchell, A.J. Freeman and M.G. Kanatzidis, J. Am. Chem. Soc. **131**, 5405 (2009).
[10] L.L. Zhao, T. Yi, J.C. Fettiger, S.M. Kauzlarich and E. Morosan, Phys. Rev. B **80**, 020404(R) (2009).
[11] T. Yi, A.P. Dioguardi, P. Klavins, N.J. Curro, L.L. Zhao, E. Morosan and S.M. Kauzlarich, Eur. J. Inorg. Chem. **2011**, 3920 (2011).
[12] P. Manuel, L.C. Chapon, S. Todorov, D.Y. Chung, J.P. Castellan, S. Rosenkranz, R. Osborn, P. Toledano and M.G. Kanatzidis, Phys. Rev. B **81**, 184402 (2010).
[13] Y. Nambu, L.L. Zhao, E. Morosan, K. Kim, G. Kotliar, P. Zajdel, M.A. Green, W. Ratcliff, J.A. Rodriguez-Rivera and C. Broholm, Phys. Rev. Lett. **106**, 037201 (2011).
[14] A.B. Karki, G.T. McCandless, S. Stadler, Y.M. Xiong, J. Li, Julia Y. Chan and R. Jin, Phys. Rev. B **84**, 054412 (2011).
[15] L. Buravov and J. F. Shchegolev, Prib. Tekh. Eksp. **2**, 171 (1971).
[16] N.P. Ong, Jour. Appl. Phys. **48**, 2935 (1977).
[17] Y. Trudeau, M. Poirier and A. Caillé, Phys. Rev. B **46**, 169 (1992).
[18] M. Poirier, M. Castonguay, A. Revcolevschi and G. Dhalenne, Phys. Rev. B **52**, 16058 (1996).
[19] B. Dumoulin, P. Fronzse, M. Poirier, A. Revcolevschi and G. Dhalenne, Synthetic Metals **86**, 2243 (1997).
[20] I. Nowik, I. Felner, A. B. Karki, R. Jin, Phys. Rev. B **84**, 212402 (2011).
[21] J. Pouget, in *Low-Dimensional Elctronic Properties of Molybdenum Bronzes and Oxides*, edited by C. Schlenker (Kluwer Academic, Netherlands, 1989), pp. 87-157.
[22] M. Poirier, A. Caillé and M.L. Plumer, Phys. Rev. B **41**, 4869 (1990).
[23] M. Poirier, M. Castonguay, A. Revcolevschi and G. Dhalenne, Phys. Rev. B **66**, 054402 (2002).